

EXHIBIT 1

CONFIDENTIAL

Orienting Cancellous Bone For The Preparation of Graftech Cervical Spacer

Todd Boyce, 10/9/00

Objective: Cut the bone such that the loading direction of the Cervical Spacer is in alignment with that of the tissue in the original donor bone.

Concept: When cancellous bone is formed (in the donor bone), it is aligned along the direction of loading. This put the cancellous bone is the best location and orientation to support loads in the likely loading directions.

Load is transferred from the articular surface (covered with cartilage, where it forms a joint with another bone) through this cancellous bone to the cortical shell where it is carried to the other end. Certain early researchers, including John Koch (1917), noticed distinctive patterns in the proximal femur, and found through engineering calculations that stresses within femur corresponded to the architecture of the cancellous bone (Figure 1). The body naturally places bone where it will be loaded, and removes it from places that it will not be loaded. We want to take advantage of this naturally strong orientation to make the cuts for the Cervical Spacer.

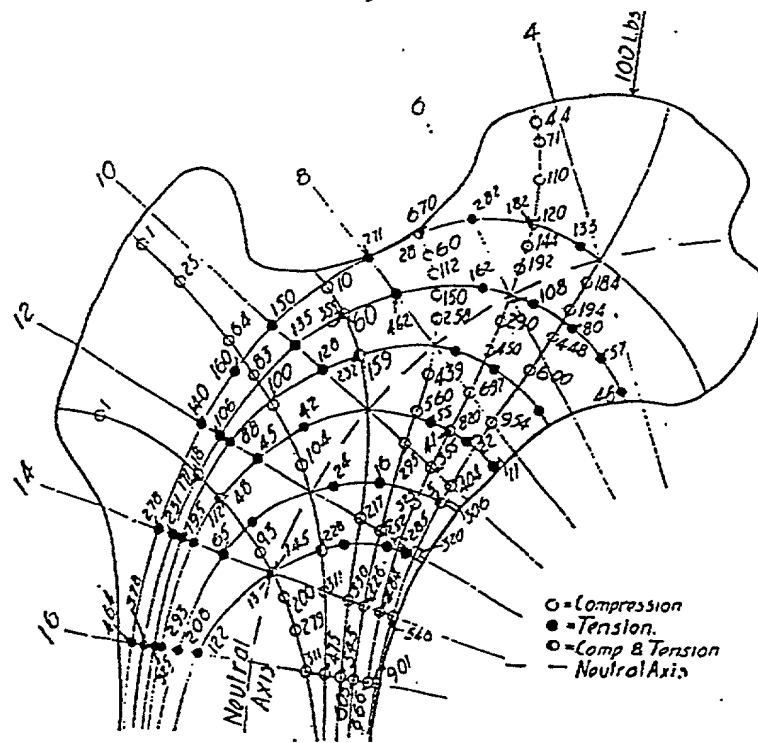
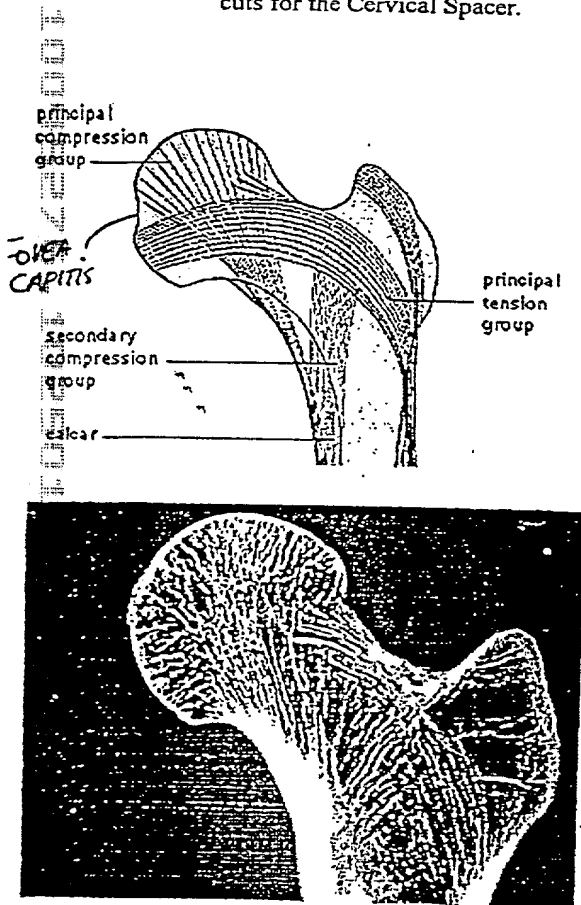


Fig. 19 a Intensity of the maximum tensile and compressive stresses in the femur-head. Computed for the load of 100 pounds on the right femur. Corresponds to the upper part of figure 18.

Figure 1 – Cancellous bone orientation in the proximal femur, and corresponding stress calculations by John Koch, 1917.

The key to cutting bones to hold orientation is to make the first, facing cuts (which will become the top or bottom surface of the Cervical Spacer) perpendicular to the trabecular orientation in the bone. This is usually perpendicular to the long axis of the bone.

Proximal Femur

The cut is made perpendicular to the principal compressive group of trabeculae (Figure 2).

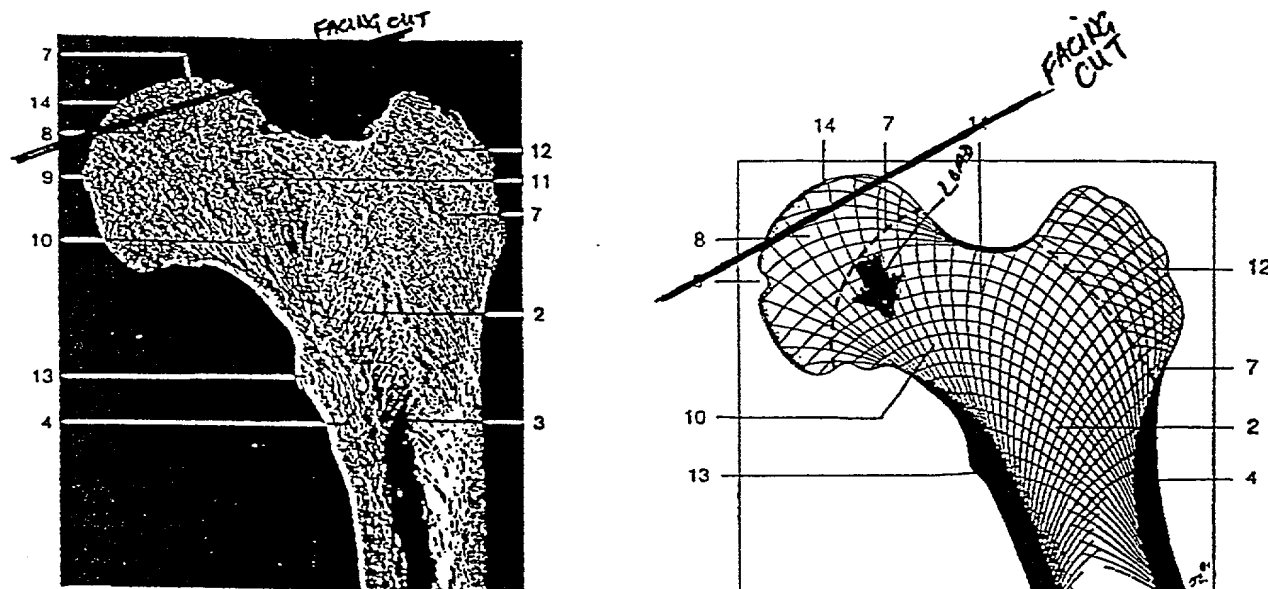


Figure 2 – Proximal femur, showing trabecular orientation and facing cut. The cut surface will then become the upper or lower surface of the finished Cervical Spacer.

Distal Femur

The facing cut for the distal femur cuts across the protrusions of the condyles (Figure 3).

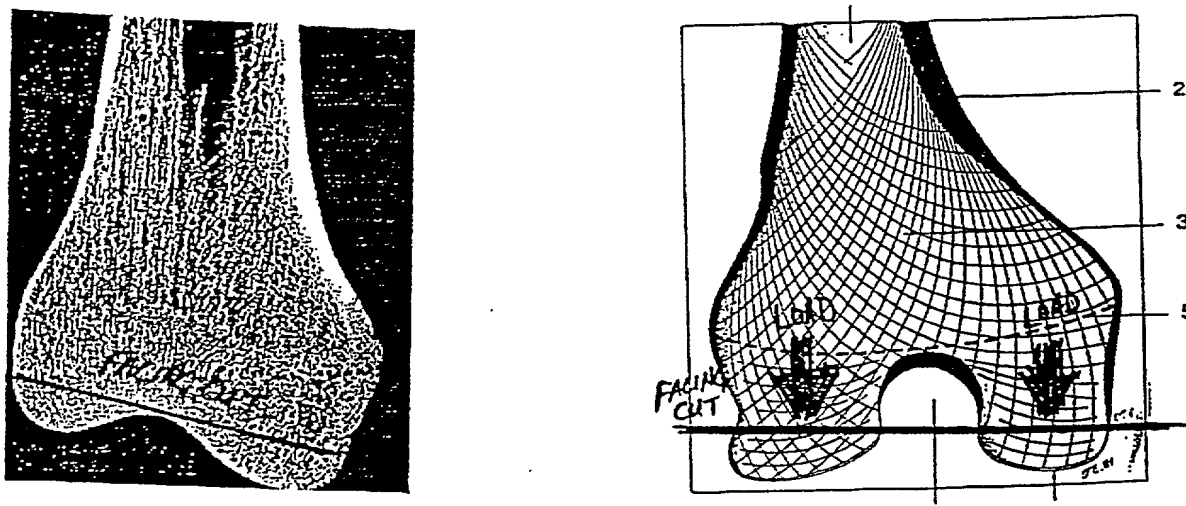


Figure 3 – Distal Femur, showing cancellous orientation and facing cut.

10045276-102501

Proximal and Distal Tibia

The tibia is loaded axially along the length of the bone, so that a standard transverse facing cut is appropriate for both the proximal and the distal ends (Figure 4).

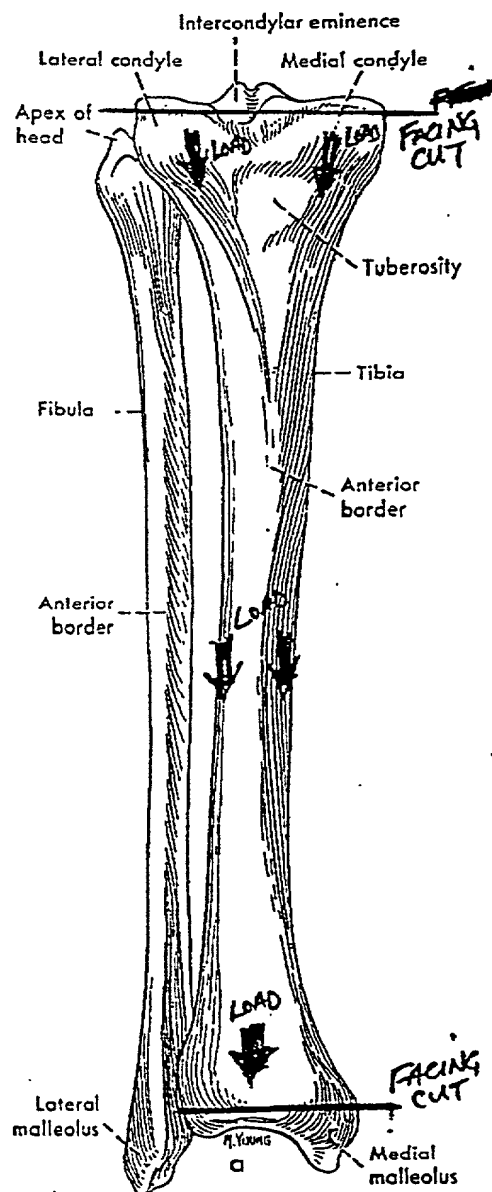
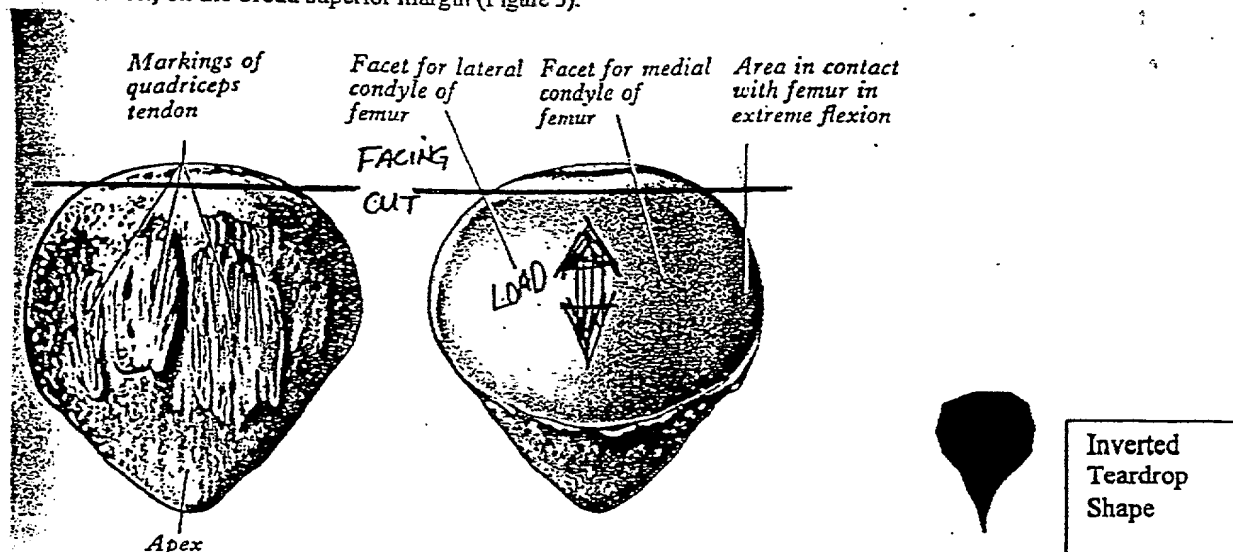


Figure 4 -- Tibia, showing facing cuts for the proximal and distal locations.

Patella

The patella is a bone that is loaded primarily in tension, between the quadriceps femoris tendon and the patellar ligament. The facing cut should transverse the patella near the insertion of the quadriceps femoris tendon, on the broad superior margin (Figure 5).



Right knee in extension

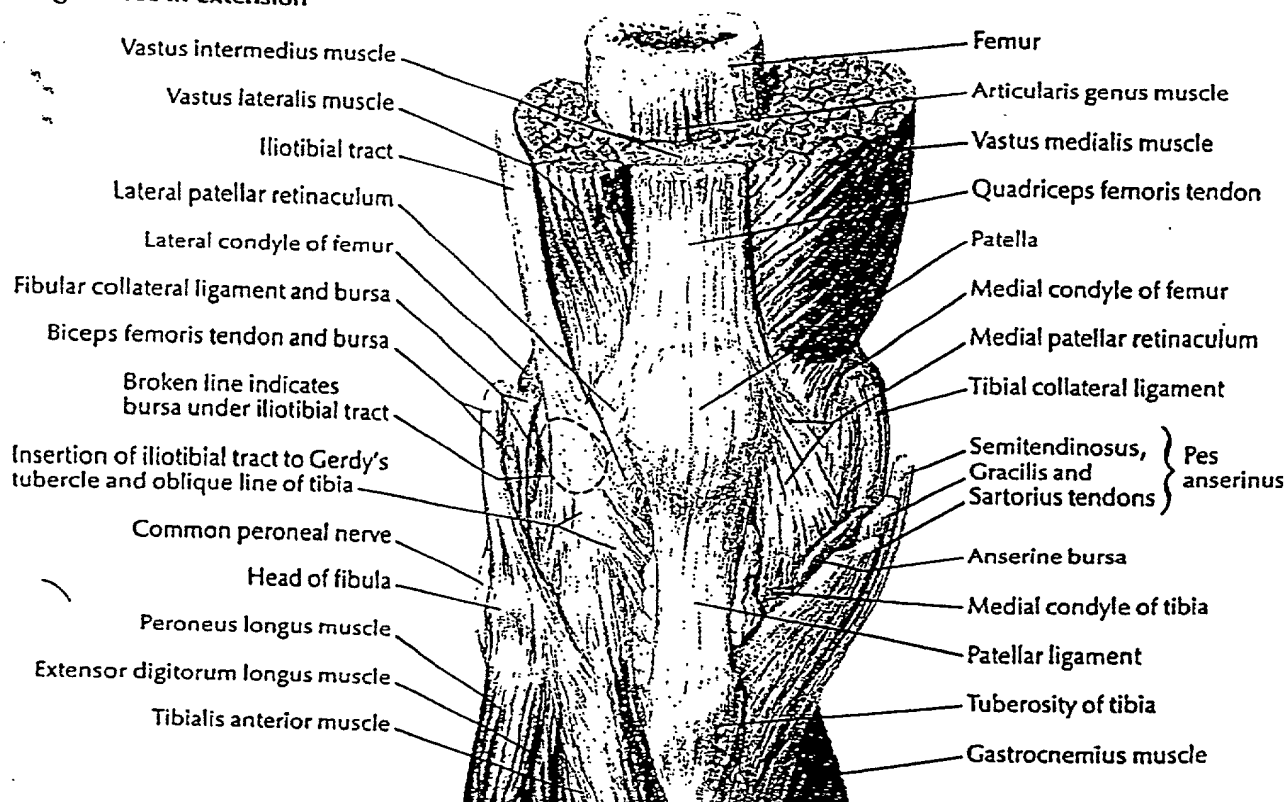
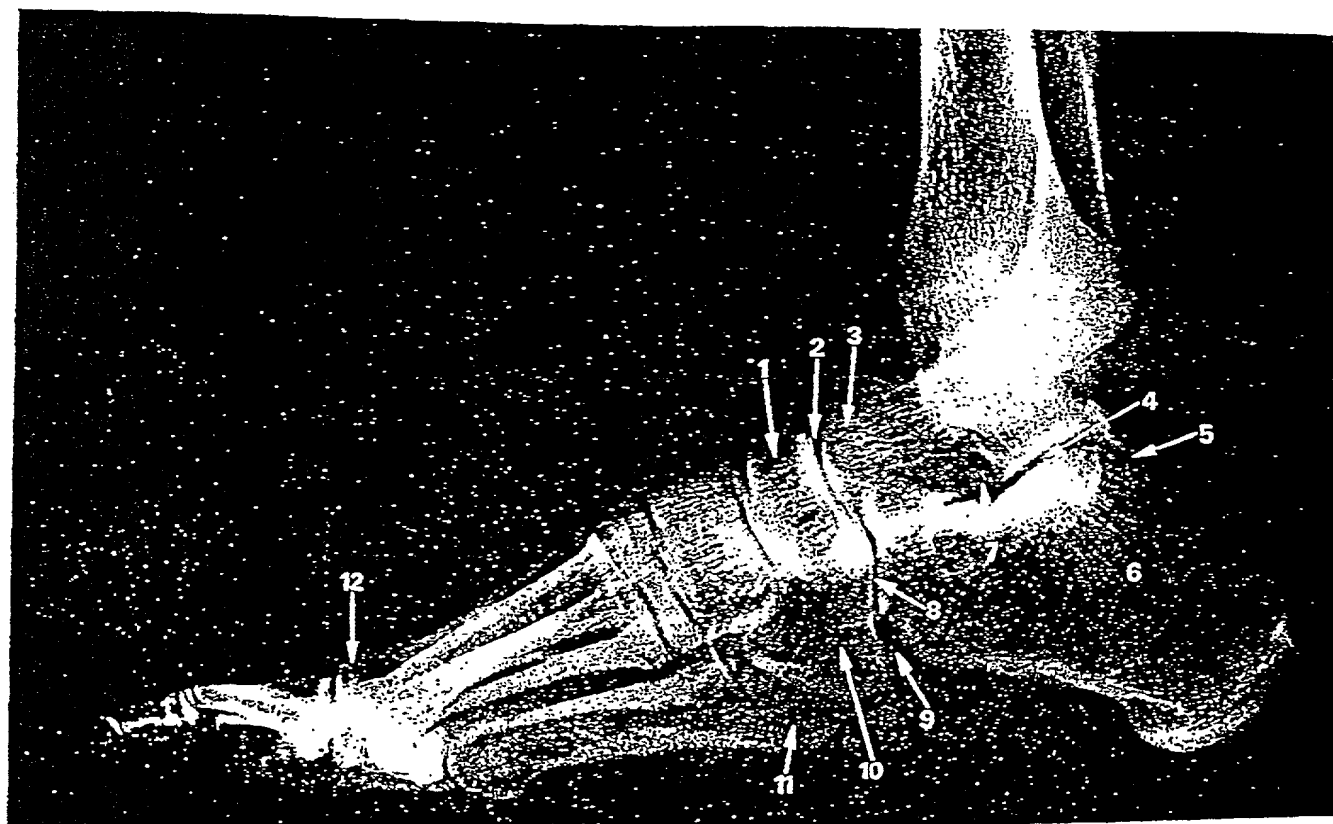


Figure 5 – Facing cuts and anatomy for the Patella.

The Foot - Talus & Calcaneus

Trabecular patterns and load distribution are shown in figure 6 for a fully articulated foot, including Talus and Calcaneus.



F. Netter M.D.
© 1984 GEIGY

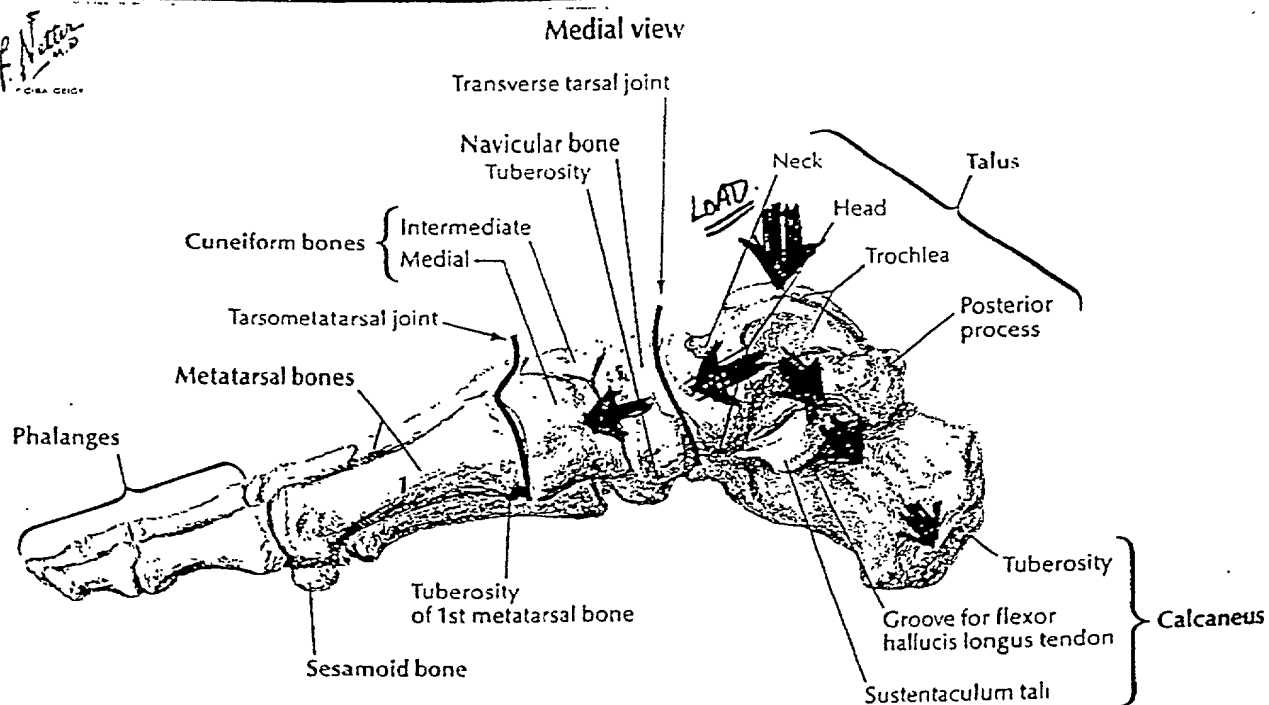


Figure 6 - Load distribution and trabecular patterns for the foot.

Talus

The talus is somewhat unique, in that the load is distributed from one articular surface to two others. Figure 6 shows cancellous trabeculae beginning from the convex superior (trochlear) surface, and then oriented toward both the convex navicular surface and the concave calcaneal surface. Facing cuts can be made from any of these three surfaces and still allow appropriate trabecular orientation (Figure 7). As before, the surface made by the facing cuts becomes either the upper or lower surface of the Cervical Spacer.

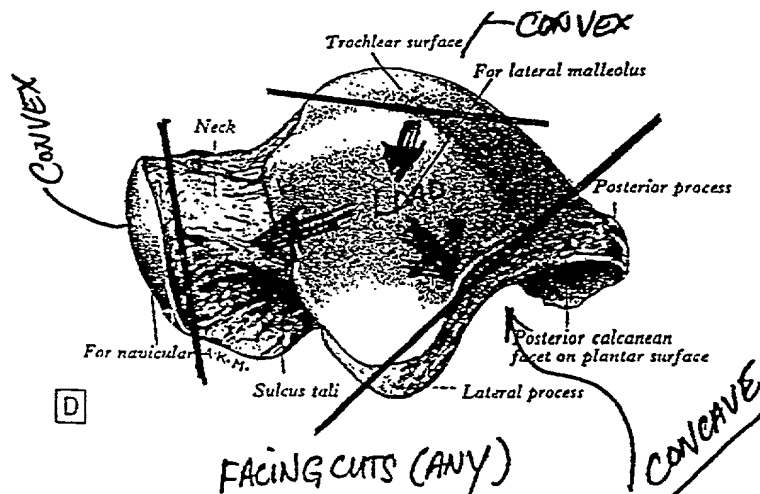


Figure 7 – Facing cuts and loading distribution for the Talus.

Calcaneus

The calcaneus is loaded along its long axis from the joint made with the Talus (Figure 6). Facing cuts can be made from the talar surface, or from the tip, or heel region (Figure 8).

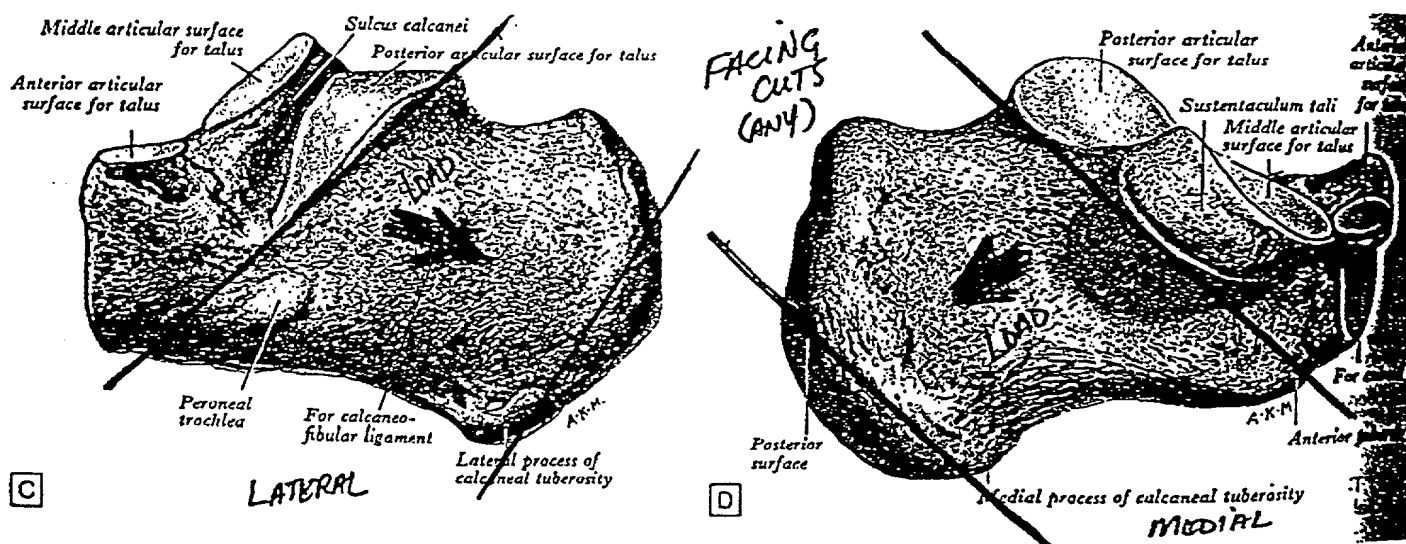


Figure 8—Calcaneal loading and facing cuts.

Humerus

The load on the humerus is approximately along the long axis, thus facing cuts are approximately perpendicular to the long axis.

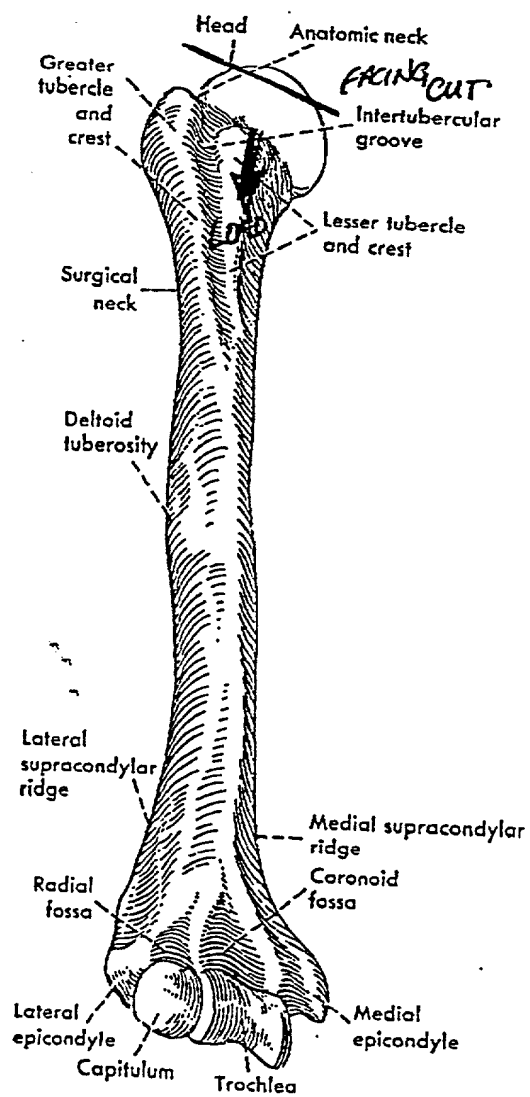


Figure 6-2. Anterior (a) and post

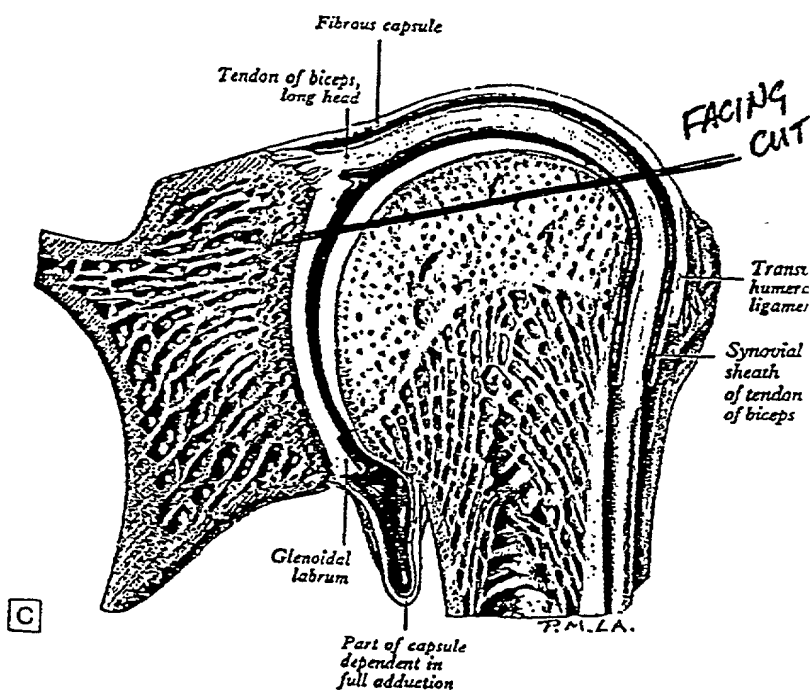
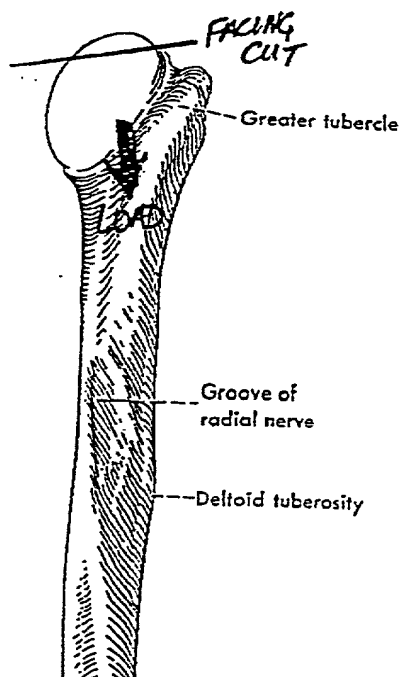


Figure 9 - Humerus, showing loading orientation and facing cut.

Additional points:

- Note that in almost every case, the facing cut is made parallel to an articular (cartilage) surface.
- Additional cuts can be made beneath the original facing surface (wafering), as long as they are cut parallel to the original facing cut, and the bone is strong enough (by the pinch test, and other methods that will be defined later).
- Once the cervical spacers are blanked, it is important that you be able to re-establish the right orientation to make the finishing cuts. Develop a systematic method of orienting or marking the cervical spacer blanks so that you can re-orient them easily and accurately for the final machining steps.

10046376 103604




























TYPE OF JOINT AND ITS LOADING	BONE	CORONAL SECTION	SAGITTAL SECTION	TRANSVERSE SECTION
Primary spongiosa - growth structure	Metaphyses			
PRESSURE SYSTEMS				
UNI-DIRECTIONAL LOADING	Vertebral body			
MULTI-DIRECTIONAL LOADING a) concave surface	Acetabulum			
b) convex joint surface epiphysis	Femoral head			
c) convex joint surface metaphysis	Femoral neck			
ONE-PLANE LOADING Uniaxial joint a) concave surface	Lower tibia			
b) convex surface	Upper tibia			
BILATERAL BENDING	Lumbar vertebra-spinous process			
TENSION SYSTEMS				
	Patella			

Fig. 17. Scheme of different types of cancellous bone architecture. Tension systems dashed.

EXHIBIT 2

CONFIDENTIAL

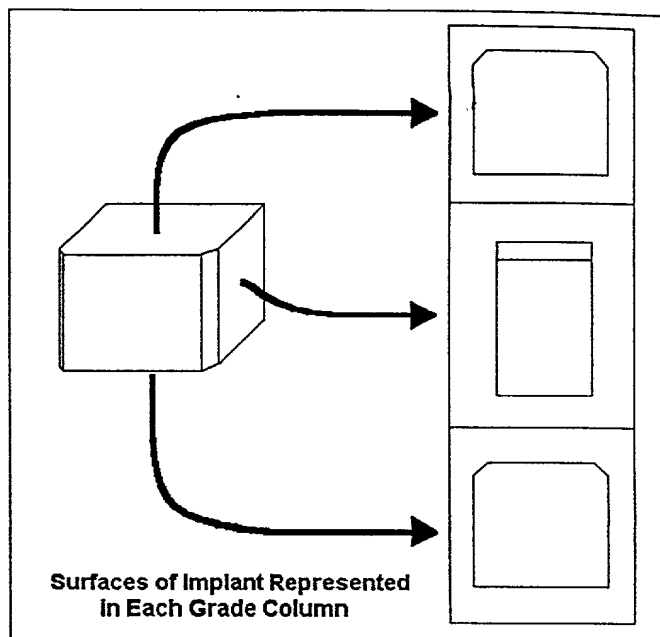
Freeze-Dried Graftech Cervical Spacer: Implant Visual Grade Characteristics

Grade 1:

- All flat surfaces have a uniform appearance and show very little porosity.
- Where visible, pores are very small and do not penetrate deeply into the implant.
- All implant edges are sharp and well defined.
- Very little or no discernable visual variation in density throughout the implant.

Grade 2:

- Some flat surfaces of the implant appear slightly more porous than in Grade 1.
- Pores are small and do not penetrate deeply into the implant.
- Most implant edges are sharp and well defined, with some showing slight serration when passing through small pores.
- Overall porosity is only slightly more than in Grade 1 and distributed fairly evenly throughout the surface of the implant.



Grade 3:

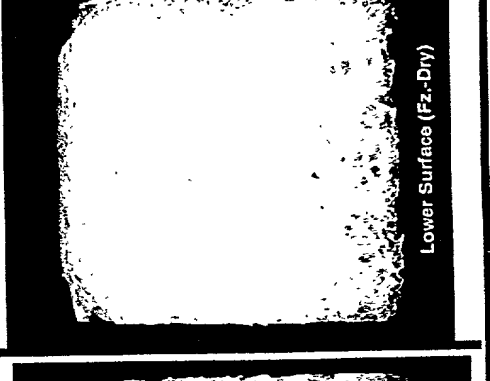
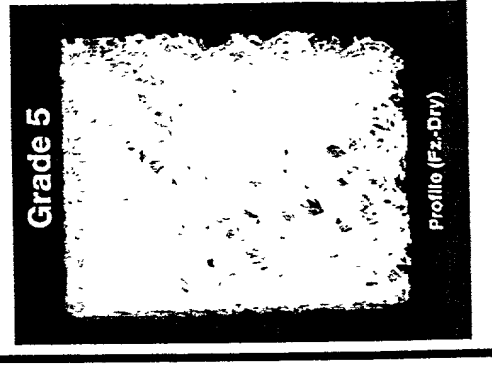
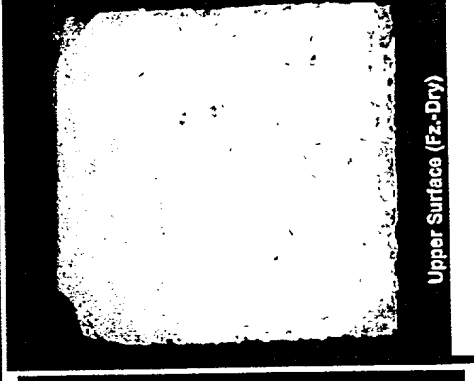
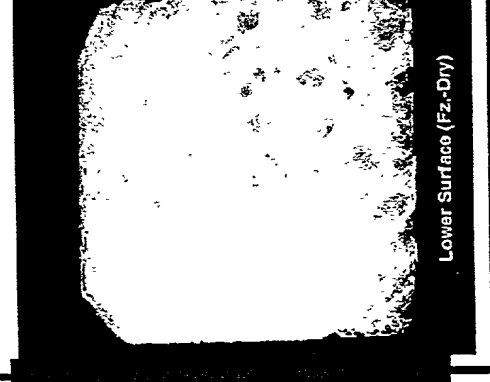
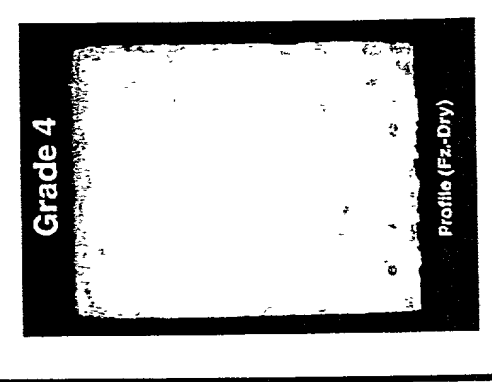
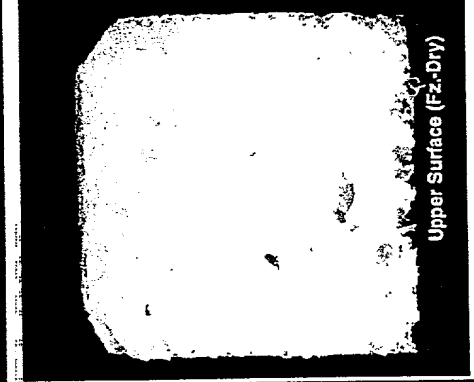
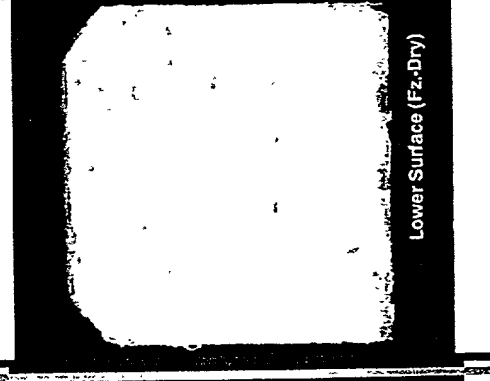
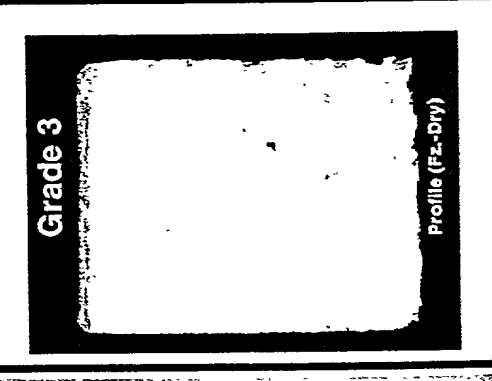
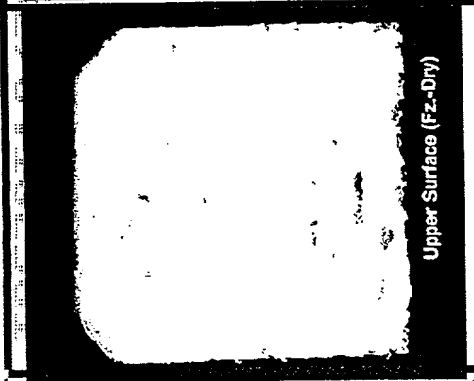
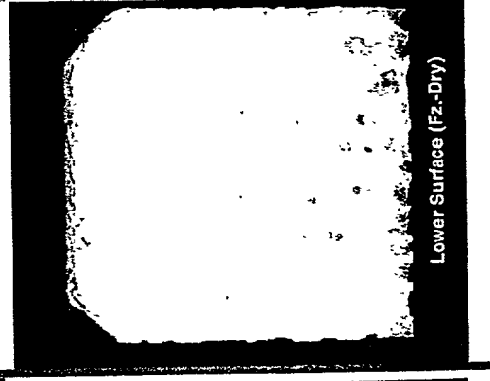
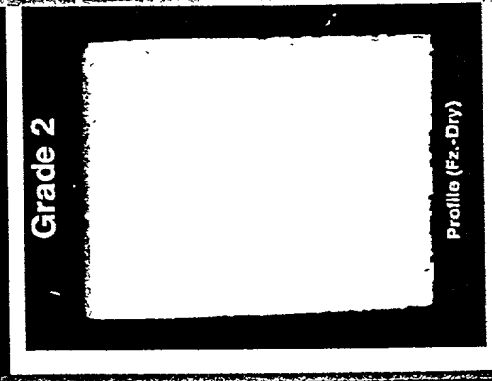
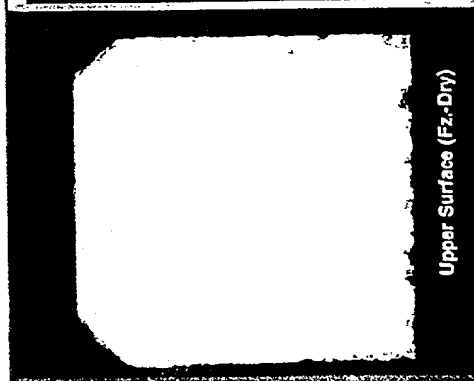
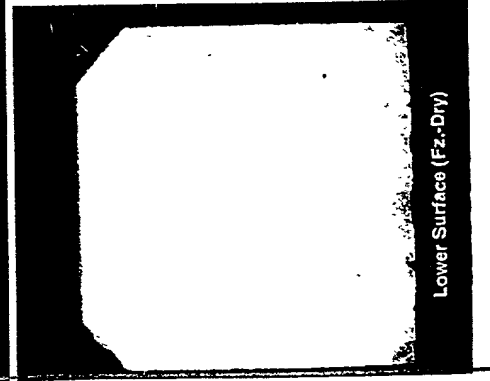
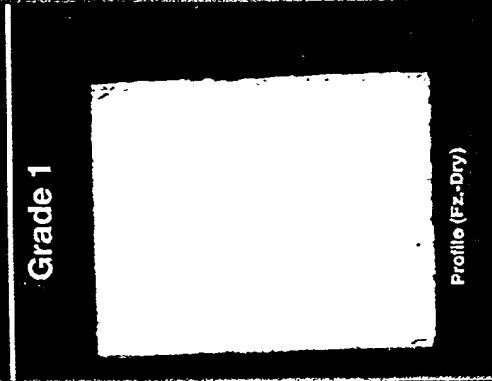
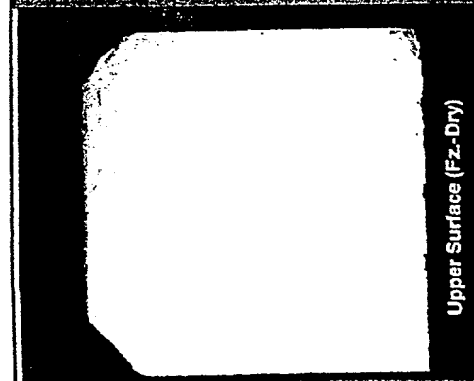
- Pores on flat surfaces are slightly larger, vary more in size and shape, and are distributed more unevenly than in Grade 2.
- Edges tend to be less well defined. Some edges have a wavy appearance due to passing through larger size pores.
- Overall implant porosity is not uniform in appearance. Some regions of the implant are noticeably more porous in appearance than others.
- In some regions of the implant, pores are larger and reach deeper into the implant than in Grade 2.

Grade 4:

- Pores on flat surfaces are larger and deeper than those described in Grade 3.
- Large pores are present over the majority of the implant surface.
- Edges and corners are not well defined and tend to be rounded in appearance.
- Most edges are interrupted where crossing large pores.
- Pores on flat surfaces appear to be more prevalent than bone. Edges of the implant appear translucent.
- Majority of the implant's surface has a web-like appearance. Implant looks fragile.

Grade 5:

- Pores are so large and more prevalent than bone that the surfaces and body of the implant has a net-like appearance.
- Body of implant appears to be almost transparent.
- Edges are not well defined and have small thread-like protrusions. Chamfer edges are very hard to discern.
- Implant looks extremely fragile.



Study Report: Graftech Cervical Spacer (ACF)
Machine-Cut Size Effects - Density vs. Strength
(00-068)

DRAFT

Prepared By: John Winterbottom _____ Date _____
Associate Scientist, Research and Development

Copies to:

Implant Systems: Jo-Wen Lin
Development Engineer, Implant Systems

R&D: Todd Boyce
Scientist, Research & Development

Regulatory: Chris Talbot
Director, Regulatory Affairs

QA: Ted Buriani
Director, Quality Assurance

Marketing: Greg Maxwell
Director, Bio-Implants Product Development

Jennifer Stone
Product Manager, Spinal Systems

Purpose of Study

The main objectives of this study were to:

- Mechanically test the largest and smallest sizes of the proposed ACF implants in static compression, using the results to determine if statistically significant differences exist in their load carrying characteristics.
- Develop a linear regression between freeze-dried apparent density and compressive strength for the largest and smallest sizes of the proposed ACF implant.
- Determine whether or not the linear relationship between freeze-dried apparent density and compressive strength is significantly influenced by the size of the implant being considered.

Materials and Methods

Specimens belonging to the following two groups were tested in compression:

- 11mm x 14mm x 5mm (L x W x H), V.I. treated, freeze-dried, machine-cut ACF dense cancellous
- 11mm x 14mm x 13mm (L x W x H), V.I. treated freeze-dried, machine-cut ACF dense cancellous

Specimens derived from 5 different donors were used for this study. It should be noted that all of the test articles used in this study were cut by machine.

Test specimens were placed in physiological saline at room temperature for 30 minutes prior to testing. Compressive tests were each performed as quickly as possible, but no more than 5 minutes from the time that each test article is removed from the saline fluid.

Specimens were preloaded (under load control) to 10 N of compressive load. Machine axial displacement was then zeroed at this preload.

The testing equipment used was the MTS model 858 Bionix materials testing system. The system load cell (± 100 kN) operated in the ± 10 kN load range, and the system actuator-mounted LVDT were used to collect load and displacement information. Testworks version 4 software was used for load displacement data acquisition and storage and machine control.

Specimens were loaded using a ramp waveform at a constant rate of 25 mm/minute in displacement control mode. A total displacement of 3 mm was applied to the 11x14x13mm test articles and a total displacement of 2mm was applied to articles in the 11x14x5mm group.

John Winterbottom, Associate Scientist, conducted these tests at Osteotech Inc. Headquarters, located in Eatontown, NJ.

Terminology

The terms "density" and "calculated density" throughout this report refer to apparent density calculated from the measured weights and dimensions presented in the Appendix. The term "nominal density" refers to apparent density calculated using specimen weight and the nominal dimensions for that implant size (e.g. volume calculated using 11x14x5mm with 2.11mm chamfer).

The term "absolute error" refers the absolute value of the difference between a regression equation prediction for a specimen load at yield value, and the actual load at yield value obtained from the compressive testing of that specimen.

Results

Tests were performed in accordance with the protocol¹ approved on 8/15/00. The following tables and figures summarize the results for both size groups included in the study:

Table 1: Individual Results for 11x14x5 Specimens

Specimen Number	Load At Yield N	Extension At Yield mm	Calculated Density (g/cc)	Nominal Density (g/cc)
1A	2420.8	0.3626	0.7154	0.7648
2A	1441.4	0.4317	0.6046	0.6425
3A	1082.4	0.3378	0.5666	0.6070
4A	1815.8	0.3790	0.6209	0.6651
5A	1561.0	0.2767	0.6321	0.6542
6A	1960.6	0.2052	0.6572	0.6862
7A	1485.1	0.4222	0.6336	0.6838
8A	1145.4	0.4599	0.5311	0.5583
9A	1116.9	0.3635	0.5236	0.5597
10A	1102.5	0.4039	0.5071	0.5408
11A	1478.5	0.4209	0.5844	0.6041
12A	680.4	0.3618	0.3840	0.3965
13A	497.6	0.3266	0.5527	0.6046
14A	3501.4	0.4228	0.8470	0.9229
15A	3174.1	0.2670	0.7872	0.8613
16A	896.0	0.4757	0.7114	0.7750
17A	715.5	0.3876	0.5901	0.6457
18A	2798.7	0.2670	0.7221	0.7857
19A	1005.9	0.3608	0.7522	0.8153
20A	3098.1	0.3237	0.8526	0.9184
21A	3256.6	0.3792	0.8105	0.8766
22A	3470.1	0.2545	0.7465	0.8207
23A	3558.2	0.2545	0.8072	0.8797
24A	1611.7	0.2180	0.5708	0.6179
25A	1347.2	0.2216	0.4820	0.5205
26A	1493.6	0.3470	0.5449	0.5757
27A	2547.3	0.3213	0.6879	0.7479
28A	1124.2	0.2204	0.5541	0.5908
29A	805.6	0.2224	0.5108	0.5347
30A	1235.7	0.2041	0.6280	0.6739
Mean	1780.9	0.3300	0.6373	0.6843
Std. Dev.	953.8	0.0817	0.1178	0.1333

Table 2: Individual Results for 11x14x13 Specimens

Specimen Number	Load At Yield N	Extension At Yield mm	Calculated Density (g/cc)	Nominal Density (g/cc)
1B	1876.9	0.3510	0.6875	0.7199
2B	2576.3	0.4487	0.6365	0.6733
3B	1383.1	0.4171	0.6336	0.6618
4B	1964.6	0.3750	0.7168	0.7492
5B	2331.2	0.4188	0.6301	0.6606
6B	1360.2	0.3060	0.5514	0.5697
7B	831.9	0.9466	0.4054	0.4133
8B	656.7	0.3632	0.4588	0.4813
9B	1578.2	0.6423	0.5642	0.5934
10B	1095.2	0.4748	0.5048	0.5331
11B	869.9	0.4021	0.4613	0.4825
12B	845.0	0.4345	0.4943	0.5162
13B	1107.7	0.3034	0.5570	0.5890
14B	2173.5	0.3793	0.7350	0.7772
15B	2673.0	0.5197	0.7955	0.8557
16B	1596.5	0.3216	0.6380	0.6607
17B	1905.1	0.4318	0.6876	0.7270
18B	901.6	0.3465	0.5872	0.6260
19B	1605.9	0.3749	0.5200	0.5429
20B	1683.1	0.3342	0.7518	0.8004
21B	1693.2	0.4482	0.6607	0.6974
22B	1278.3	0.3760	0.4782	0.5039
23B	1570.6	0.4015	0.6541	0.6957
24B	1422.3	0.3125	0.6902	0.7274
25B	1707.8	0.4621	0.7881	0.8284
26B	2247.4	0.4684	0.7431	0.7810
27B	1434.6	0.5720	0.6739	0.7281
28B	1287.7	0.4672	0.5867	0.6316
29B	532.1	0.2229	0.4962	0.5202
30B	700.2	0.2395	0.5269	0.5507
Mean	1496.3	0.4187	0.6105	0.6433
Std. Dev.	565.6	0.1338	0.1061	0.1152

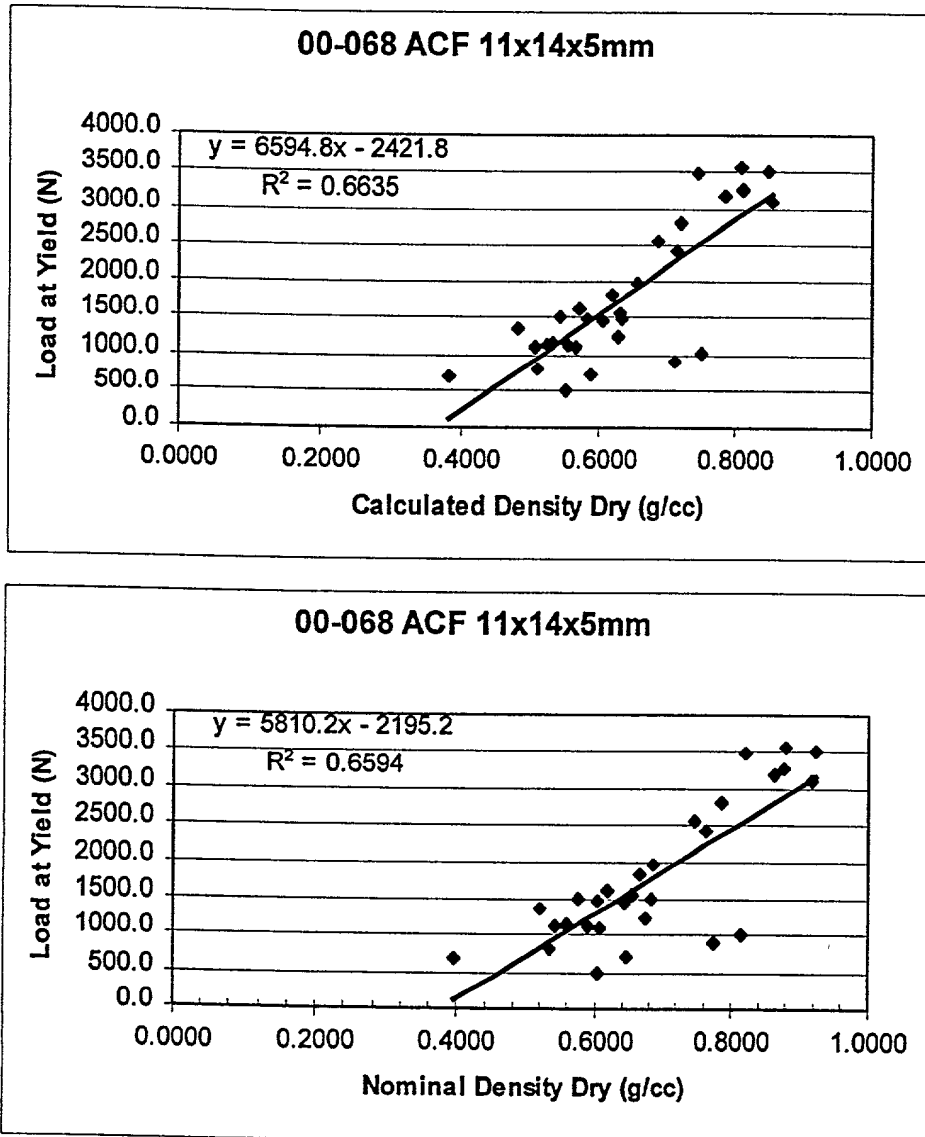


Figure 1: Load at Yield Scatter Plots for the 11x14x5mm Group

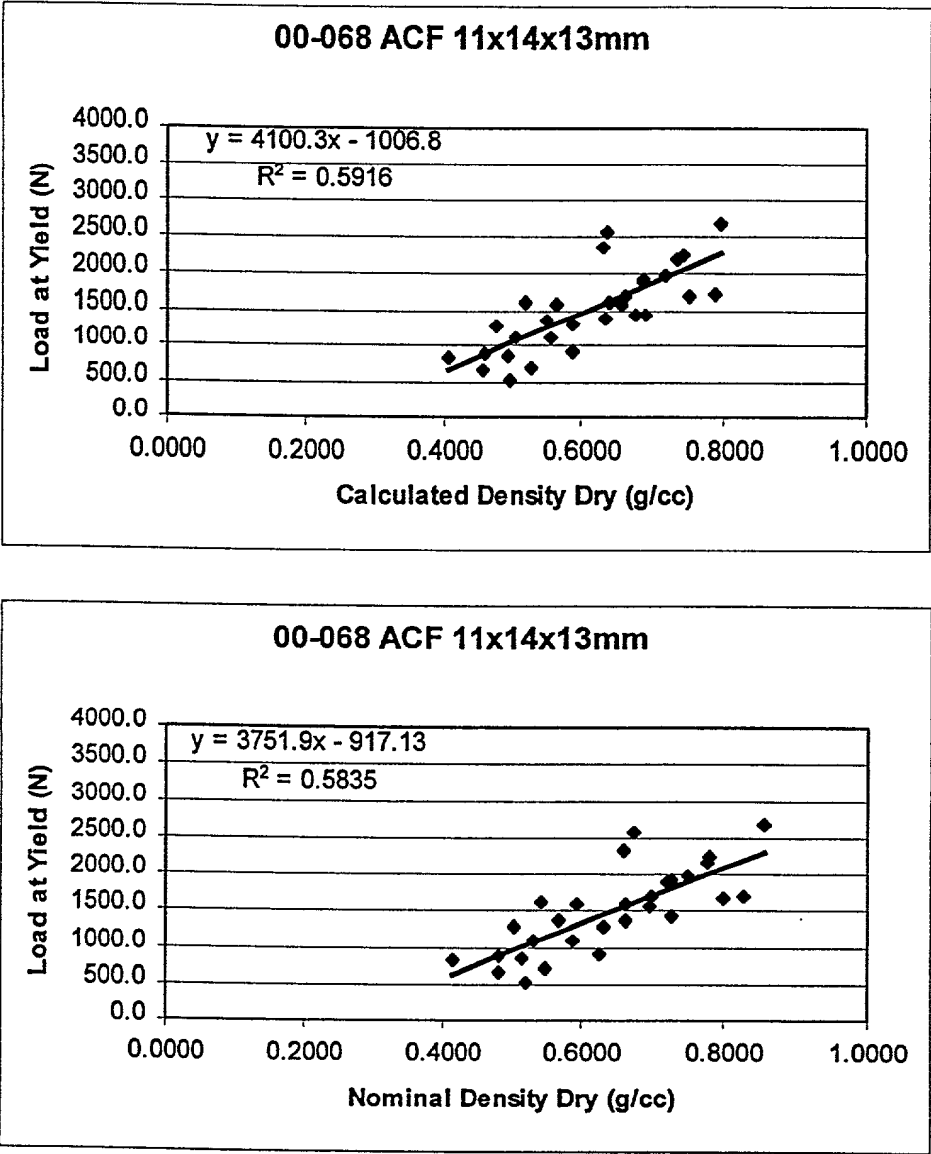


Figure 2: Load at Yield Scatter Plots for the 11x14x13mm Group

Table 3: Two-Sample t-Test Assuming Equal Variances, Load at Yield

	11x14x5mm	11x14x13mm
Mean (N)	1780.9	1496.3
Variance	909769.5	319942.1
Observations	30	30
Pooled Variance	614855.8	
Hypothesized Mean Difference	0	
df	58	
t Stat	1.4057	
P(T<=t) one-tail	0.0826	
t Critical one-tail	1.6716	
P(T<=t) two-tail	0.1651	
t Critical two-tail	2.0017	

Table 4: Two-Sample t-Test Assuming Equal Variances, Displacement at Yield

	11x14x5mm	11x14x13mm
Mean (mm)	0.3300	0.4187
Variance	0.0067	0.0179
Observations	30	30
Pooled Variance	0.0123	
Hypothesized Mean Difference	0	
df	58	
t Stat	-3.10035	
P(T<=t) one-tail	0.00149	
t Critical one-tail	1.67155	
P(T<=t) two-tail	0.00298	
t Critical two-tail	2.00172	

Table 5: Comparison of Load at Yield Means for Hand-Cut and Machine-Cut Specimens, Differing in Cross-Sectional Area

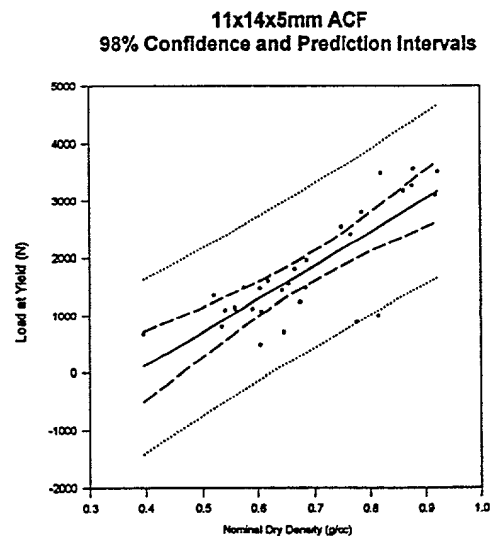
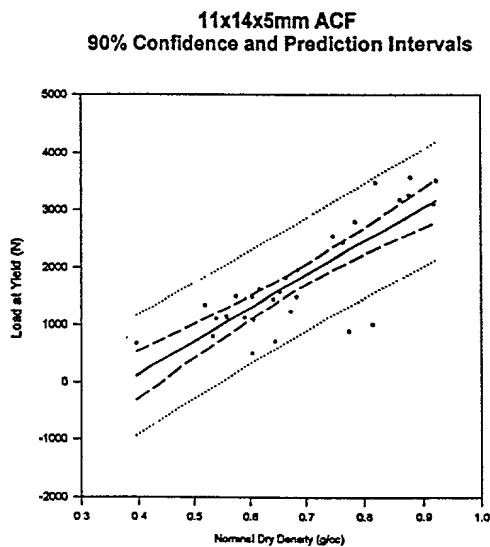
	11x14x5 (068)	11x11x5 (063)
Mean (N)	1780.9	1426.3
Variance	909769.5	293973.4
Observations	30	31
Pooled Variance	596652.9	
Hypothesized Mean Difference	0	
df	59	
t Stat	1.7929	
P(T<=t) one-tail	0.0391	
t Critical one-tail	1.6711	
P(T<=t) two-tail	0.0781	
t Critical two-tail	2.0010	

Table 6: Summary of Absolute Error Calculations for Differing Prediction Types

Prediction Type Reg. Eqn. predicts Population	Average Absolute Error (N)	Sum of Absolute Error (N)
13mm predicts 13mm	282	8458
All 068 predicts 13mm	298	8946
5mm predicts 13mm	345	10353
5mm predicts 5mm	403	12075
All 068 predicts 5mm	427	12810
13mm predicts 5mm	484	14532

Table 7: Two-Sample t-Test Assuming Equal Variances, Cross-Prediction Absolute Error

	5mm Predicts 13mm	13mm Predicts 5mm
Mean (N)	345.1	484.4
Variance	68414.0	160008.7
Observations	30	30
Pooled Variance	114211.3	
Hypothesized Mean Difference	0	
df	58	
t Stat	-1.5968	
P(T<=t) one-tail	0.0579	
t Critical one-tail	1.6716	
P(T<=t) two-tail	0.1158	
t Critical two-tail	2.0017	

**Figure3: Load at Yield Scatter Plots with Confidence and Prediction Intervals for 11x14x5mm ACF**

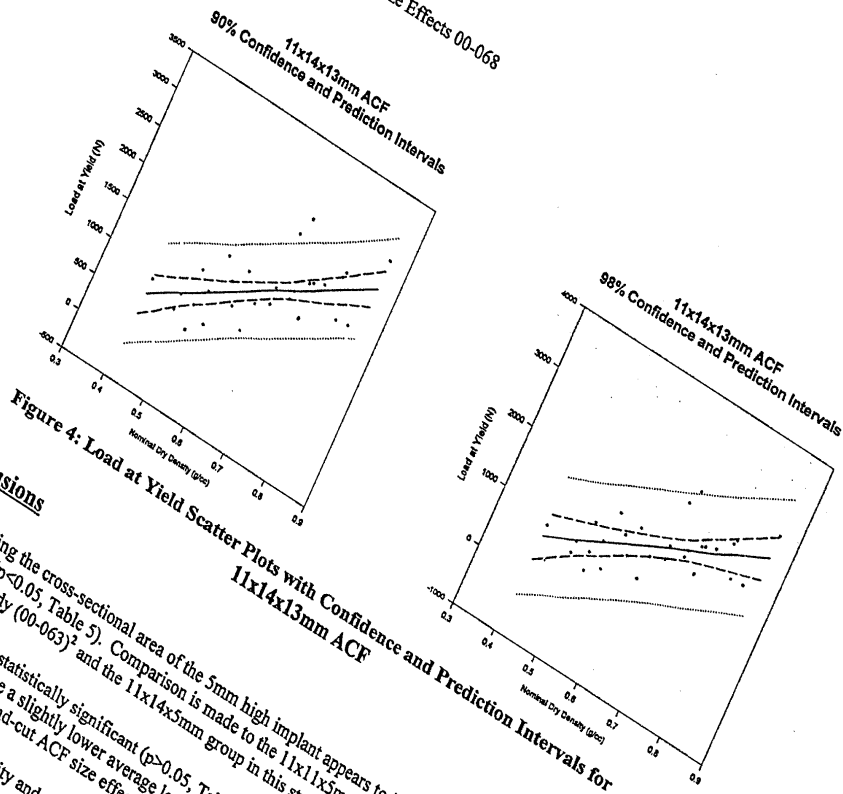


Figure 4: Load at Yield Scatter Plots with Confidence and Prediction Intervals for 11x14x13mm ACF

Conclusions

- Increasing the cross-sectional area of the 5mm high implant appears to increase the compressive load at yield ($p < 0.05$, Table 5). Comparison is made to the 11x11x5mm group in the hand-cut ACF effects study (00-063) and the 11x14x5mm group in this study.
- Although not statistically significant ($p > 0.05$, Table 3), there appears to be a trend for the larger height values for smaller hand-cut and smaller machine-cut specimens were 0.63 and 0.66 respectively. Values for r^2 in the larger sized implant groups for hand-cut and machine-cut specimens, were 0.18 and 0.58 respectively. Thus, for both implant size extremes, machine-cut specimens had stronger density to load at yield relationships.
- For both groups tested in this study, dry weight of the specimen would be essentially as predictive of strength as would calculated dry density. Note the small change in r^2 values between nominal density and calculated density vs. load at yield (Figures 1 and 2).
- For both test groups, the difference in average absolute error between a regression equation predicting its own size group, and the cross-prediction on the same group (e.g. 5mm predicts 5mm vs. 13mm predicts 5mm) was 63N and 81N. This indicates that the cross-prediction ability for different sized machine-cut specimen regression equations is only slightly worse than the predictive ability of the regression equation derived directly from that group.
- Absolute error averages in cross-prediction were not significantly different ($p > 0.05$) between the two size groups (Table 7).

Documents Referenced

1. "Study Protocol: Graftech Cervical Spacer (ACF) Size Effects - Density vs. Strength (00-068)", Osteotech Inc., 8/15/00
2. Study Report: Hand-Cut Bio-ACF Size Effects – Density vs. Strength (00-063), Osteotech Inc.

1004936-100001

Appendix**11x14x5mm Specimens**

Specimen Number	Dry wt. (g)	W	Freeze-Dry Dim (mm)			Wet wt. (g)
			D	T	C	
1A	0.5719	13.46	11.26	5.41	1.95	0.8157
2A	0.4804	13.48	11.21	5.4	1.99	0.6851
3A	0.4539	13.59	11.3	5.36	2.03	0.7131
4A	0.4973	13.51	11.36	5.37	2.08	0.703
5A	0.4892	13.42	11.19	5.29	1.97	0.7186
6A	0.5131	13.42	11.24	5.31	1.95	0.7208
7A	0.5113	13.52	11.48	5.34	2.02	0.7985
8A	0.4175	13.56	11.09	5.36	1.93	0.6233
9A	0.4185	13.56	11.36	5.33	2.02	0.5909
10A	0.4044	13.48	11.37	5.35	2.05	0.5777
11A	0.4517	13.51	11.01	5.33	1.93	0.6135
12A	0.2965	13.49	11.11	5.29	1.98	0.4125
13A	0.4521	13.69	11.43	5.36	1.97	0.7367
14A	0.6901	13.63	11.39	5.39	2.02	0.9639
15A	0.644	13.53	11.51	5.39	1.99	0.9553
16A	0.5795	13.77	11.28	5.39	2.05	0.8495
17A	0.4828	13.64	11.47	5.36	1.95	0.751
18A	0.5875	13.5	11.49	5.39	2.04	0.8423
19A	0.6096	13.62	11.52	5.3	2	0.874
20A	0.6867	13.57	11.43	5.34	2.07	0.9322
21A	0.6555	13.55	11.5	5.32	1.95	0.9056
22A	0.6137	13.67	11.48	5.38	2.03	0.8267
23A	0.6578	13.6	11.57	5.31	1.97	0.9231
24A	0.462	13.52	11.46	5.36	1.98	0.6494
25A	0.3892	13.59	11.4	5.34	1.93	0.6348
26A	0.4305	13.57	11.37	5.25	1.95	0.7543
27A	0.5592	13.65	11.53	5.31	2.07	0.8759
28A	0.4418	13.55	11.41	5.31	2.11	0.7321
29A	0.3998	13.57	11.33	5.24	2.09	0.7025
30A	0.5039	13.57	11.43	5.32	2.07	0.7949
Mean	0.511713	13.55967	11.366	5.34	2.004667	0.755897
S.D.	0.099678	0.078717	0.140433	0.042508	0.052898	0.128361

1004936-10501

11x14x13mm Specimens						
	Dry wt. (g)	W	D	T	C	Wet wt. (g)
1B	1.3996	13.52	11.43	13.55	2.07	2.1905
2B	1.3090	13.52	11.48	13.65	2.13	2.4164
3B	1.2867	13.52	11.40	13.55	2.06	1.9529
4B	1.4566	13.57	11.35	13.52	1.93	2.202
5B	1.2842	13.53	11.39	13.56	1.95	2.3185
6B	1.1076	13.53	11.22	13.54	1.86	2.066
7B	0.8035	13.56	11.53	12.98	1.91	1.2182
8B	0.9357	13.62	11.35	13.53	1.96	1.4653
9B	1.1536	13.56	11.47	13.55	2.15	1.7205
10B	1.0365	13.53	11.43	13.64	2.03	1.5012
11B	0.9381	13.63	11.32	13.55	2.05	1.4747
12B	1.0036	13.55	11.31	13.60	1.99	1.5586
13B	1.145	13.65	11.38	13.57	1.96	2.1268
14B	1.5109	13.63	11.38	13.60	1.99	2.3367
15B	1.6636	13.65	11.51	13.64	1.95	2.551
16B	1.2844	13.29	11.39	13.68	2.05	2.0297
17B	1.4134	13.58	11.40	13.62	1.97	2.3757
18B	1.2171	13.58	11.48	13.66	2.04	2.1676
19B	1.0554	13.51	11.34	13.61	2.02	1.8207
20B	1.556	13.59	11.52	13.57	2.01	2.2806
21B	1.3559	13.56	11.48	13.55	2.05	1.9399
22B	0.9797	13.56	11.39	13.61	1.98	1.4293
23B	1.3526	13.58	11.49	13.62	2.05	1.883
24B	1.4141	13.54	11.48	13.53	2.00	2.0934
25B	1.6105	13.60	11.32	13.65	2.06	2.4965
26B	1.5183	13.60	11.36	13.61	2.09	2.4276
27B	1.4155	13.63	11.55	13.68	1.97	2.1853
28B	1.228	13.63	11.50	13.71	2.02	1.8588
29B	1.0113	13.53	11.35	13.62	1.98	1.9487
30B	1.0706	13.55	11.27	13.63	1.91	1.9538
Mean	1.250567	13.56333	11.409	13.57933	2.006333	1.999663
S.D.	0.223891	0.066661	0.082602	0.124067	0.065257	0.352698

10946276 109501